The Effects of E_rxB Flow Shear Profile on the Formation of Internal Transport Barrier in ITER

Thawatchai Onjun
Plasma and Fusion Research Unit, Sirindhorn International Institute of Technology,
Thammasat University, Pathum Thani, 12121, Thailand

Abstract

An improvement of nuclear fusion performance in ITER tokamak with an internal transport barrier (ITB) is investigated. Self-consistent simulations of ITER in the standard *H*-mode scenario with the presence of an ITB are carried out using a 1.5D BALDUR integrated predictive modeling code. In these simulations, a version of the Mixed Bohm/gyro-Bohm (Mixed B/gB) core transport model that includes ITB effects is used to compute the evolution of plasma profiles. In this transport model, the transport in the core region can be stabilized by the influence of $E_r \times B$ flow shear and magnetic shear. To illustrate the *H*-mode plasma properties, the boundary conditions in these simulations are described using the pedestal temperature model based on the magnetic and flow shear stabilization width concept, together with the infinite-*n* ballooning stability concept. The combination of Mixed B/gB transport model with ITB effects, together with the pedestal model, is used to simulate the time evolution of temperature, density, and current profiles for the ITER plasmas. The presence of ITB results in complicated scenarios, that can yield improved performance, compared with standard *H*-mode discharges. It is found that the formation of ITBs has a strong impact on both electron and ion temperature profiles, especially near the center of the plasma; while only small impact is found on the electron density. When the effect of an ITB is not included, the predicted central ion temperature is just above 10 keV. With an ITB included in the simulation, the central ion temperature can significantly increase up to the range of 30 keV, depending on the details of $E_r \times B$ flow shear profile. The increase of central temperature results in a significant improvement in the alpha power production and, consequently, the fusion performance. It is observed that the thermal and particle diffusivities in most of the plasma core are smaller in the simulations with an ITB included than in those without the ITB. This reduction in the diffusivity results in stronger gradients and, consequently, higher values of the central temperature and density.

Keywords: Fusion, Plasma, Tokamak, *H*-mode, ITER, ITB, ETB

1. Introduction

In order to achieve a significant fusion reaction rate inside a nuclear fusion reactor, the ability to heat and contain high temperature plasmas inside the reactor is strongly required. Since the high confinement mode (*H*-mode) discharge [1] in tokamaks generally yields excellent energy confinement and has acceptable particle transport rates for impurity control, future nuclear fusion experiments such as the International Thermonuclear Experimental Reactor (ITER) [2], which aim to demonstrate the scientific and technological

feasibility of nuclear fusion energy using the magnetic confinement fusion concept, are designed to operate in the *H*-mode regime. It has been widely observed in many experiments from various tokamaks that the performance of an *H*-mode discharge can be further improved with the formation of a transport barrier inside the plasma, called an internal transport barrier (ITB) [3]. In general, the formation of an ITB is associated with the $E_r \times B$ flow shear. The presence of an ITBs due to $E_r \times B$ flow shear in *H*-mode plasmas is likely to result in an improved scenario that yields higher plasma temperatures and, consequently, fusion power production, which is more suitable for future nuclear fusion experiments.

In recent years, predictions of ITER performance in the standard type I ELMy *H*-mode scenario using integrated predictive modeling codes have been intensively studied [4-12]. For example, the BALDUR integrated predictive modeling code with Mixed Bohm/gyroBohm (Mixed B/gB) and MMM95 anomalous core transport models were used to predict the performance of ITER [4, 6-8]. The performance of ITER was evaluated in terms of the nuclear fusion power production and the fusion *Q*, which is the ratio of fusion power (to neutrons and alpha particles) to the applied auxiliary heating power. A wide range of performance is predicted, depending on the choice of plasma density, heating power, impurity concentration and assumptions about the core transport models employed in the simulations. In the recent work by T Onjun *et al*. [6, 7], the simulations of ITER were carried out with Mixed B/gB and MMM95 core transport model and different edge transport barriers ETB models. It was found in all ETB models that the predicted performance of ITER with Mixed B/gB model is relatively low (Fusion $Q \sim 3$) compared to those simulations using MMM95 model (Fusion $Q \sim 10$). It is worth noting that the BALDUR simulations using Mixed B/gB and MMM95 models agree equally well with present-day experiments [13, 14]. In the ITER study using JETTO code with Mixed B/gB model [5], an optimistic performance of ITER was found (Fusion $Q \sim 16$ with $T_{ped} \sim 5$ keV). An access to second stability of ballooning mode instability for the plasma edge was obtained, and it was responsible for an increase of the pedestal temperature and, consequently, the central temperature, and the fusion performance. In Refs. [9, 10], PTRANSP code with GLF23 core transport model was used to simulate ITER performance. A wide range of performance was also found with the Fusion *Q* of 5-14. A recent report from the International Tokamak Physics Activity (ITPA) Profile Database group using PTRANS and ASTRA codes to investigate fusion performance in ITER was published in reference [11]. It was found that in the ELMy H-mode scenario, a wide range of Fusion *Q* was found (ranges from 5.5 to 20.1). Note that a pedestal temperature of 5.6 keV, predicted using Sugihara model [15], was used in the PTRANS simulations while the pedestal temperature of 1 keV was used in ASTRA simulations. It can be concluded that a wide range of fusion *Q* was observed, with the minimum fusion *Q* obtained below the target Fusion *Q* (Fusion *Q* of 10). Note that the effects of ITBs have not been included in the simulations in the previous studies. In Ref.[12], it showed that the presence of ITB can significantly improve the ITER performance. Because the formation of ITB depends sensitively on the $E_r \times B$ flow shear, it is consequently important to explore ITER scenarios with different forms of $E_r \times B$ flow shear.

It is widely known that the presence of ITBs usually results in an improved plasma performance, especially near central temperature and density. In general, the presence of ITBs results in a peaking of plasma profiles in the ITB region. The physics of ITBs can be found in Ref. [3].

There are several models attempting to describe formation of ITBs [16-18]. An original Mixed B/gB model was modified to include the effect of ITBs by suppression of anomalous core transport using E_rxB flow shear and magnetic shear. This model has been successfully reproduced in many experiments from large tokamaks in various scenarios [17, 19-22].

In this paper, a study of ITER simulations is presented that includes the effects of an ITB in the *H*-mode plasma. In general, a formation of edge transport barriers (ETB) is a key signature of *H*-mode plasma, which is responsible for improved properties of *H*-mode plasma. In this work, the ETB is described in terms of a pedestal model based on magnetic and flow shear stabilization width scaling and a pressure gradient by a ballooning mode instability criterion [23]. In simulations of discharges that contain an ITB, the ITB is formed by the suppression of core anomalous transport by the influence of $E_r \times B$ flow shear and magnetic shear. In this work, the $E_r \times B$ flow shear is obtained directly from either JET discharge 40542 or JET discharge 40847.

This paper is organized as follows: brief descriptions of relevant components of the BALDUR code, the anomalous transport model, and the pedestal model are presented in Section 2; predictions of ITER performance using the BALDUR code are described in Section 3; and a summary is given in Section 4.

2. BALDUR Code

The BALDUR integrated predictive modeling code is used to compute the time evolution of plasma profiles including electron and ion temperatures, deuterium and tritium densities, helium and impurity densities, magnetic q ($\equiv \frac{m}{n}$, where m is the toroidal rotation around the torus and n is the poloidal rotation around the torus), and densities of neutrals and fast ions. These time-evolving profiles are computed in the BALDUR code by combining the effects of many physical processes self-consistently, including the effects of transport, plasma heating, particle influx, boundary conditions, the plasma equilibrium shape, and sawtooth oscillations. Fusion heating and helium ash accumulation are also computed self-consistently. BALDUR simulations have been intensively compared with a wide variety of plasma experimental data, which yield an overall agreement with about a 10% relative RMS deviation [13, 14]. In the BALDUR code, fusion heating power is determined by the nuclear reaction rates together with a Fokker Planck package used to compute the slowing down spectrum of fast alpha particles on each flux surface in the plasma. The fusion heating component of the BALDUR code also computes the rate of the production of thermal helium ions and the rate of the depletion of deuterium and tritium ions within the plasma core. The effect of sawtooth oscillation is taken into account using the Porcelli sawtooth model [24] to trigger sawtooth crashes and a modified Kadomtsev magnetic reconnection model [25] to describe the effects of each sawtooth crash.

2.1 Model for ITB

In this work, an ITB is formed by the suppression of core anomalous transport due to ω_{ExB} flow shear and magnetic shear. This effect is included in the Mixed Bohm/gyro-Bohm (Mixed B/gB) anomalous core transport model [26]. It was originally a local transport model with Bohm scaling. A transport model is said to have "Bohm" scaling when the transport diffusivities are proportional to the gyro-radius times thermal velocity. Transport diffusivities in models with Bohm scaling are also functions of the profile shapes (characterized by normalized gradients) and other plasma parameters such as magnetic *q*. These parameters are held fixed in

systematic scans in which only the gyro-radius is changed relative to plasma dimensions. The original model was subsequently extended to describe ion transport, and a gyro-Bohm term was added in order to produce simulation results that match data from smaller tokamaks as well as data from larger machines. A transport model is said to have "gyro-Bohm" scaling when the transport diffusivities are proportional to the square of the gyro-radius times thermal velocity divided by a plasma linear dimension, such as the major radius. The Bohm contribution to the original model usually dominates over most of the plasma. The gyro-Bohm contribution usually makes its largest contribution in the deep core of the plasma, and it plays a significant role only in smaller tokamaks with relatively low heating power and low magnetic field. To include the ITB effect, the Bohm contribution is modified by a cut-off that is a function of magnetic and flow shear. The Bohm/gyro-Bohm transport model with ITB effect included [17] can be expressed as follows:

$$\chi_e = 1.0\chi_{gB} + 2.0\chi_B$$

$$\chi_i = 0.5\chi_{gB} + 4.0\chi_B$$

$$D_H = D_Z = \left[0.3 + 0.7\rho\right]\frac{\chi_e\chi_i}{\chi_e + \chi_i}$$

where

$$\chi_{gB} = 5\times10^{-6}\sqrt{T_e}\left|\frac{\nabla T_e}{B_\phi^2}\right|$$

$$\chi_B = 4\times10^{-5}R\left|\frac{\nabla\left(n_eT_e\right)}{n_eB_\phi}\right|q^2\left(\frac{T_{e,0.8}-T_{e,1.0}}{T_{e,1.0}}\right)$$

$$\Theta\left(-0.14 + s - \frac{1.47\varpi_{E\times B}}{\gamma_{ITG}}\right)$$

In these expressions, χ_e is the electron diffusivity, χ_i is the ion diffusivity, D_H is the particle diffusivity, D_z is the impurity diffusivity, χ_{gB} is the gyro-Bohm contribution, χ_B is the Bohm contribution, ρ is normalized minor radius, T_e is the local electron temperature in keV, B_T is the toroidal magnetic field, R is the major radius, n_e is the local electron density, q is the safety factor, s is the magnetic shear [r (d q / dr) / q], ω_{ExB} is the E_rxB flow shear, C_{ExB} is the constant for E_rxB flow shear effect (in most of simulations, C_{ExB}=1), and γ_{ITG} is the ITG growth rate, estimated as v_{ti}/qR, in which v_{ti} is the ion thermal velocity. The role of impurity transport is very complicated and crucial for burning plasma experiments, since it controls impurity behaviour, such as helium ash accumulation. Since the original Mixed B/gB model does not include impurity transport, in this work, it is assumed that the impurity transport is equal to the particle transport. Note that most notations used in this paper are described in Table 1.

Table 1: Notation used in this paper

Symbol	Unit	Description
ρ		Normalized minor radius
T_e	keV	Local electron temperature
R	m	Major radius
a	m	Minor radius
I_p	MA	Plasma current
B_ϕ	Tesla	Toroidal magnetic field
$n_{e,20}$	X10^{20} m^{-3}	local electron density
q		Safety factor
s		Magnetic shear
ω_{ExB}	s^{-1}	E_rxB flow shear
γ_{ITG}	s^{-1}	ITG growth rate
T_{ped}	(keV)	Pedestal temperature
n_{ped}	m^{-3}	Pedestal density
M	AMU	Hydrogenic mass
α_c		Normalized critical pressure gradient

2.2 Model for ETB

In the BALDUR code, the outer

plasma boundary condition is set at the top of the pedestal. As a result, the code requires a model for both temperature and density at the top of the pedestal. A simple model for estimating pedestal temperature has been developed by using the values of pedestal width and pedestal pressure gradient [23]. In the present work, the pedestal width (Δ) is estimated using a magnetic and flow shear stabilization concept ($\Delta = C_w \rho s^2$), and the pedestal gradient is estimated using a first ballooning mode pressure gradient limit. The effects of the bootstrap current and plasma geometry are also considered. The pedestal temperature takes the following form:

$$T_{ped}(keV) = 0.323 C_W^2 \left(\frac{B_\phi}{q^2}\right)^2 \left(\frac{M}{R^2}\right) \left(\frac{\alpha_c}{n_{ped,19}}\right)^2 s^4,$$

where $n_{\mathrm{ped},19}$ is the electron density at the top of the pedestal in units of 10^{19} m^{-3}. The expression used to compute the normalized critical pressure gradient, α_c, and the calibration used to determine the constant C_W (=2.42) are described in Ref. [23]. In general, the pedestal density (n_{ped}) in *H*-mode plasmas is a large fraction of line average density (n_l). Here the pedestal density is taken to be:

$$n_{ped} = 0.71 n_l$$

based on the model employed in Ref. [4].

3. Results and Discussions

The BALDUR code is used to carry out simulations of ITER with the design parameters for full-current standard type I ELMy *H*-mode discharges (R = 6.2 m, a = 2.0 m, I_p = 15 MA, B_T = 5.3 T, κ_{95} = 1.7, δ_{95} = 0.33 and n_l = 1.0x10^{20} m^{-3}). In the simulations, the plasma current and density are slowly ramped up to the target values within the first 100 seconds of the simulation, shown in Fig 1. The plasma current during the startup phase is initially 3 MA and is slowly increased at the rate of 0.12 MA/sec to the target current. It is found, using the pedestal module [27], that the plasma makes a transition to the *H*-mode phase at 4 sec during this startup ramp. In this work, the threshold for the transition from *L*-mode to *H*-mode occurs when the plasma heating power exceeds the following empirical expression for the threshold power, taken from [2]:

$$P_{L\to H}[MW] = 2.84 M_{AMU}^{-1} B_\phi^{0.82} n_{e,20}^{-0.58} R^{1.00} a^{0.81}.$$

It is worth noting that there are several physical processes that have not been included in these simulations, such as ELM crashes and neoclassical tearing modes. Consequently, the simulation results do not represent the complete dynamic behavior of the ITER plasma. However, it is expected that these simulations include enough physics to describe the plasma, when it reaches a quasi-steady state with sawtooth oscillations. The simulations yield complex and interesting interactions within the plasma itself — such as the self heating of the plasma by the production of fast alpha particles and redistribution of heating power after each sawtooth crash. Sawtooth oscillations are considered during the simulations. For each simulation, the core transport is a combination of anomalous transport and neoclassical transport. An anomalous transport is calculated using the Mixed B/gB transport model with the effect of ITB included, while neoclassical transport is computed using the NCLASS module [28]. The boundary conditions are provided at the top of the pedestal by the pedestal model. In many experiments, it was found that ion pedestal temperature tends to be higher than electron pedestal temperature, especially in low density plasma. Since the ITER plasma is a high density plasma, and consequently, with high collisionality, the ion pedestal temperature should not be much different from the electron pedestal temperature. For simplicity, it is assumed in this work that the electron and ion pedestal temperatures have the same values. Note that this assumption for the ion and electron pedestal temperatures was employed in the BALDUR code to carry out the *H*-mode

simulations for present day experiments, in which the agreement between simulations and experiments was in the range of 10% RMS deviation [13, 14]. In these simulations, the total auxiliary heating power is 40 MW, which is composed of a combination of 33 MW NBI heating power together with 7 MW of RF heating power.

During the slow current ramp, the plasma density is also ramped up to the final plasma density while the full heating power is applied, starting from the beginning of the simulation. During this ramp, the plasma makes an automatic transition from *L*-mode to *H*-mode, which is considered by the power threshold model [2]. Since there is a strong heating early in the simulations, all the simulations enter the *H*-mode phase approximately within 4 sec. In Fig. 1, the E_rxB flow shear profiles for optimized magnetic shear discharges in the Joint European Torus (JET), discharges 40542 and 40847, are shown. It can be seen that the E_rxB flow shear profile from both discharges are different shapes, in which the main peaks are at $\rho = 0.2$ and $\rho = 0.6$ for JET discharge 40542 and the main peaks are at $\rho = 0.3$ and $\rho = 0.7$ for JET discharge 40847. In addition, the magnitude of E_rxB flow shear for JET discharge 40542 is larger than that for JET discharge 40847.

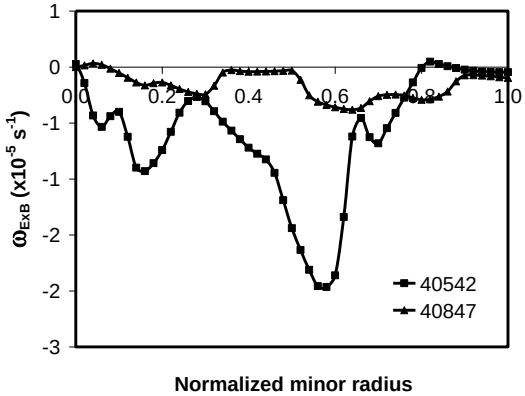

Figure 1: The E_rxB flow shear profiles for JET discharge 40452 and 40847 are plotted as a function of a normalized minor radius.

In Fig. 2, the simulated profiles for ion temperature, electron temperature, and electron density in ITER are shown as a function of normalized minor radius at a time before a sawtooth crash. These results are shown for simulations that are carried out using the Mixed B/gB model with the effects of ITB excluded and included. It can be seen that when ITB effects are included, the temperature in the region close to the plasma center increases, while the temperature near the edge remains almost unchanged. The increase of temperature in the simulation with E_rxB flow shear obtained from JET discharge 40542 is larger than that from JET discharge 40847. This increase of temperature results from the stronger temperature gradient in the region close to the plasma center. In Fig. 3, the profiles from the plasma center up to $\rho = 0.8$ of ion thermal transports from simulations when the ITB effects are included or excluded are shown. It can be seen that ion thermal transport in the region close to the plasma center in the simulations with the ITB effects included are several times smaller than that with the ITB effect excluded. This reduction of ion thermal transport results in a stronger temperature gradient in the region close to the plasma center, and consequently, an increase of central ion temperature. It can also be seen that the ITB effective region extends to a plasma radius of up to $\rho = 0.6$ in the simulation using E_rxB flow shear obtained from JET discharge 40542, and up to $\rho = 0.3$ in the simulation using E_rxB flow shear obtained from JET discharge 40847. The width of ITB effective region is associated with the location of the main peaks of E_rxB flow shear profile in Fig. 2. In addition, it can be seen that the temperature gradient in the ITB effective region in the simulation using E_rxB flow shear obtained from JET discharge 40542 is higher than that from JET discharge 40542. All in all, it can be concluded that the ITB region in the simulation using E_rxB flow shear obtained

from JET discharge 40542 has a larger ITB region and stronger temperature in the ITB region. This is not surprising since the E_rxB flow shear profile obtained from JET discharge 40542 is higher than that from JET discharge 40847.

It is also found that the pedestal boundary condition remains almost constant after the density reaches its target value. Note that the ion pedestal temperature is assumed to be the same as the electron pedestal temperature in this model. Also, the effects of ELMs have not been included in these simulations. For the electron density, the core profile is nearly flat, with relatively limited central peaking. When an ITB is included, the central density profiles from both simulations remain nearly unchanged.

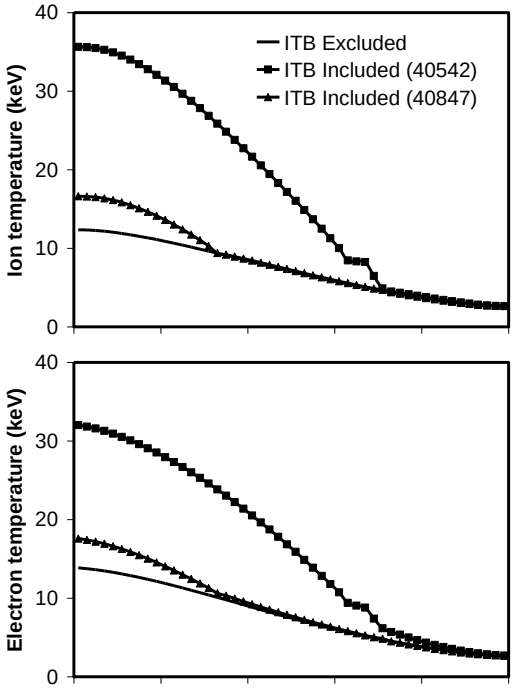

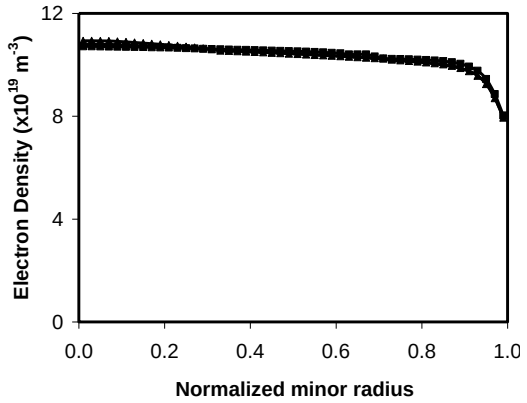

Figure 2: Profiles for ion temperature and electron temperature and electron density are plotted as a function of a normalized minor radius at the time before a sawtooth crash. The simulations are carried out with and without ITB effects.

Summaries of the average plasma parameters predicted by these simulations are shown in Table 2. It can be seen that the central ion temperature increases when the ITB effects are included. The average central ion temperature in the ITB simulation with E_rxB flow shear obtained from JET discharge 40542 is about 31.2 keV, which is in the effective range for nuclear fusion power production. The central ion temperatures increase by 160% and 20% in the simulations with the ITB effects included using E_rxB flow shear obtained from JET discharge 40542 and JET discharge 40847, respectively. This increase of central temperature has a strong impact on the total plasma stored energy and the nuclear fusion power production.

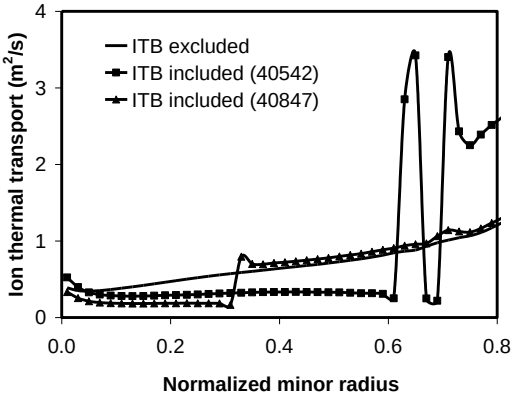

Figure 3: The profile of total ion diffusivity is plotted as a function of normalized minor radius at time of 1000 sec. The simulations are carried out with and without ITB effects.

The plasma stored energy is shown as a function of time between 900 to 1000 sec in Fig. 4. It can be seen that the plasma stored energy is in the range of 210 MJ for the simulation with no ITB, while the plasma stored energy increases to 220 MJ in simulations with the ITB effects included, using E_rxB flow shear obtained from JET discharge 40847, and increases to 430 MJ in simulations with the ITB effects included, using E_rxB flow shear obtained from JET discharge 40542. The time-dependence of the alpha power deposition is shown in Fig. 5 from the simulations with ITB effects excluded and included. It can be seen that the alpha power from the simulation with ITB effects included by using E_rxB flow shear obtained from JET discharge 40542 is much higher than that without an ITB, while the alpha power from the simulation with ITB effects included by using E_rxB flow shear obtained from JET discharge 40847 is slightly higher than that without an ITB. The average of plasma stored energy and alpha power during the time between 900 sec and 1000 sec are summarized in Table 2. The fusion performance can be evaluated in term of the fusion Q, which can be calculated as

$$\text{Fusion } Q = \frac{5 \times P_{\alpha,avg}}{P_{\text{AUX}}},$$

where $P_{\alpha,\text{avg}}$ is a time-average of the alpha power and P_{AUX} is the auxiliary heating power (equal to 40 MW for these simulations). It can be seen in Table 2 that the fusion Q increases by 420% and 20% when ITB effects are included using E_rxB flow shear obtained from JET discharge 40542 and 40847, respectively.

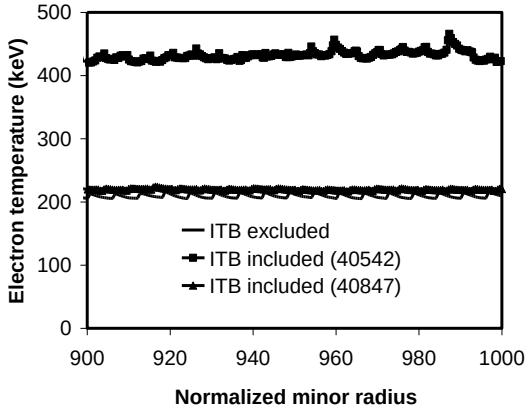

Figure 4: The plasma stored energy is plotted as a function of time for simulations with ITB effects excluded and included.

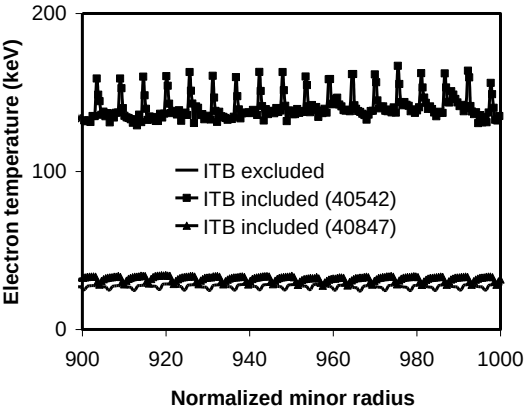

Figure 5: The alpha power production is plotted as a function of time for the simulation when an ITB is included and excluded.

Table 2: Summary of plasma parameters during last 100 sec of each simulation (from 900 sec to 1000 sec).

Parameters	Unit	ITB excluded	ITB included	
			40542	40847
$T_{i,0}$	keV	11.8	31.2	14.5
$T_{e,0}$	keV	12.9	30.0	15.5
$n_{e,0}$	10^{19} m^{-3}	10.7	10.5	10.8
T_{ped}	keV	2.6	2.6	2.6
$n_{e,ped}$	10^{19} m^{-3}	7.1	7.1	7.1
W_{tot}	MJ	209	432	219
$P_{\alpha, avg}$	MW	27.2	141	32.2
Fusion Q		3.4	17.6	4.0

In Fig. 6, the ion temperature profiles are plotted as a function of normalized minor radius for the simulation with ITB effects included by using E_rxB flow shear obtained from JET discharge 40542 and 40847. This figure aims to show the influence of E_rxB flow shear's magnitude on the prediction. It can be seen that when the values of C_{ExB} increases, the ion temperature, as well as the electron temperature, in the ITB effective region increases. In the simulations using E_rxB flow shear obtained from JET discharge 40542, the ITB effective region are the same (up to $\rho = 0.6$). On the other hand, in the simulations using E_rxB flow shear obtained from JET discharge 40847 with C_{ExB} equaling 0.5 and 1.0, the ITB effective region are the same (up to $\rho = 0.3$). However, when C_{ExB} increases to 1.5, the ITB effective region expands close to $\rho = 0.6$. In Tables 3 and 4, summaries of the average stored energy, alpha power, and fusion Q predicted by these simulations are shown. It can be seen that those parameters increase with the increasing of C_{ExB}.

Table 3: Summary of plasma parameters during last 100 sec (from 900 sec to 1000 sec) of each simulation using E_rxB flow shear obtained from JET discharge 40542 with different values of C_{ExB}.

Parameters	Unit	40542		
		C_{ExB}=0.5	C_{ExB}=1.0	C_{ExB}=1.5
W_{tot}	MJ	372	432	468
$P_{\alpha, avg}$	MW	111	141	157
Fusion Q		13.8	17.6	19.7

Table 4: Summary of plasma parameters during last 100 sec (from 900 sec to 1000 sec) of each simulation using E_rxB flow shear obtained from JET discharge 40847 with different values of C_{ExB}.

Parameters	Unit	40847		
		C_{ExB}=0.5	C_{ExB}=1.0	C_{ExB}=1.5
W_{tot}	MJ	217	219	285
$P_{\alpha, avg}$	MW	31.1	32.2	64.5
Fusion Q		3.9	4.0	8.1

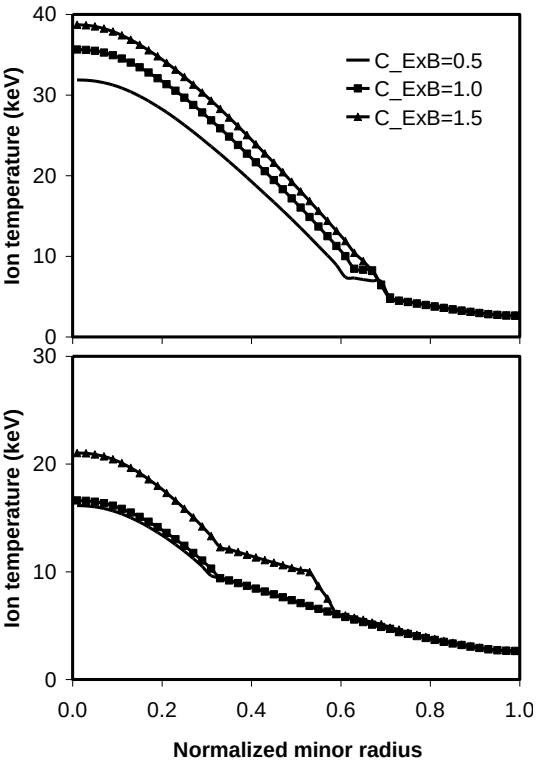

Figure 6: The ion temperature profiles are plotted as a function of normalized minor radius at the time before a sawtooth crash for different values of C_{ExB}. The simulations using ω_{ExB} from JET discharge 40542 (top) and using ω_{ExB} from JET discharge 40847 (bottom) indicate an improvement depending on values of C_{ExB}.

4. Conclusions

Self-consistent modeling of the ITER tokamak has been carried out using the BALDUR code. The outer plasma boundary in these simulations is taken to be at the top of the pedestal, where the pedestal temperatures and density are computed

using a theory-based pedestal model. The pedestal temperature model is based on magnetic and flow shear stabilization of transport together with the first stability regime of a ballooning mode limit. The pedestal temperature model is used together with a Mixed B/gB core transport model, which can include the effects of ITBs. It is found that the formation of ITBs has a strong impact on both electron and ion temperature profiles, especially near the center of the plasma; while only small impact is found on the electron density. When the effect of an ITB is not included, the predicted central ion temperature is just above 10 keV. With an ITB included in the simulation, the central ion temperature can significantly increase up to the range of 30 keV, depending of the details of $E_r \times B$ flow shear profile. The increase of central temperature results in a significant improvement in the alpha power production and, consequently, the fusion performance. It is observed that the thermal and particle diffusivities in most of the plasma core are smaller in the simulations with an ITB included than in those without the ITB. This reduction in the diffusivity results in stronger gradients and, consequently, higher values of the central temperature and density.

5. Acknowledgements

The author extends thanks to Prof. Dr. A H Kritz, Dr. G Bateman, Dr. V Parail, Dr. A Pankin, Dr. S Suwanna, Dr. N Poolyarat, and Dr. R Picha for helpful discussions and support. This work is supported by Commission on Higher Education (CHE) and the Thailand Research Fund (TRF) under Contract No. RMU5180017.

6. References

[1] Hubbard A, Physics and Scaling of the *H*-mode Pedestal, *Plasma Phys. Control. Fusion*, **42** A15, 2000.

[2] Aymar R, Barabaschi P, Shimomura Y, The ITER Design, *Plasma Phys. Control. Fusion*, **44**519, 2002.

[3] Connor J W, Fukuda T, Garbet X, *et al.*, A Review of Internal Transport Barrier, Physics for Steady-State Operation of Tokamaks, *Nucl. Fusion*, **44** R1, 2004.

[4] Bateman G, Onjun T, Kritz AH, Integrated Predictive Modelling Simulations of Burning Plasma Experiment Designs, *Plasma Phys. Control. Fusion*, **45** 1939, 2003.

[5] Onjun T, Bateman G, Kritz AH, *et al.*,Magnetohydrodynamic-Calibrated Edge-Localized Mode Model in Simulations of International Thermonuclear Experimental Reactor, *Physics of Plasmas*, **12** 082513, 2005.

[6] Onjun, T, Tharasrisuthi K, Pankin AY, *et al.*, Projected Performance of ITER Based on Different Theoretical Based Pedestal Temperature Models, *J. of Physics: Conference Series*, **123** 012034, 2008.

[7] Tharasrisuthi K, Onjun T, Onjun O, Projections of ITER Performance Based on Different Pedestal Temperature Scalings, *Thammasat International Journal of Science and Tech.*, **13** 45, 2008.

[8] Picha R, Onjun T Tharasrisuthi K, *et al.*, Dependence of ITER Performance on Pedestal Temperature, Average Electron Density, Auxiliary Heating Power, and Impurity Content, *in Proc. 35th EPS Conf on Plasma Physics, Hersonissos 9-13 June 2008*

[9] Halpern FD, Kritz AH, Bateman G, *et al.*, (Predictive Simulations of ITER Including Neutral Beam Driven Toroidal Rotation, *Phys. Plasmas*, **15** 062505, 2008.

[10] Budny RV, Andre R, Bateman G, *et al.*, Predictions of *H*-mode Performance in ITER, *Nucl. Fusion* **48** 075005, 2008.

[11] Roach CM, Walters M, Budny RV, *et al.*, The 2008 Public Release of the International Multi-tokamak Confinement Profile Database, *Nucl. Fusion* **48** 125001, 2008.

[12] Onjun T and Pianroj Y, Simulations of ITER with Combined Effects of Internal and Edge Transport Barriers, *Nucl. Fusion*, **49** 075003, 2009.

[13] Hannum D, Bateman G, Kinsey J, *et al*., Comparison of High-Mode Predictive Simulations Using Mixed Bohm/gyro-Bohm and Multi-Mode MMM95 Transport models, *Physics of Plasmas*, **8** 964 , 2001.

[14] Onjun T, Bateman G, Kritz AH, *et al*., Comparison of Low Confinement Mode Transport Simulations Using the Mixed Bohm/gyro-Bohm and The Multi-Mode-95 Transport Model, *Physics of Plasmas*, **8** 975, 2001.

[15] Sugihara M, Mukhovatov V, Polevoiet A, *et al*., Scaling of *H*-mode Edge Pedestal Pressure for a Type-I ELM Regime in Tokamaks, *Plasma Phys. Control. Fusion*, **45** L55, 2003.

[16] Zhu P, Bateman G, Kritz AH, *et al.*, Predictive Transport Simulations of Internal Transport Barriers Using the Multi-Mode Model, *Phys. Plasmas*, **7** 2898, 2000.

[17] Tala T J J, Heikkinen J A, Parail V V, *et al.*, ITB Formation in Terms of $\omega_{E\times B}$ Flow Shear and Magnetic Shear *s* on JET, *Plasma Phys. Control. Fusion*, **43** 507, 2001.

[18] Kinsey J E, Staebler GM, Waltz RE, Predicting Core and Edge Transport Barriers in Tokamaks Using the GLF23 Drift-wave Transport model, *Phys. Plasmas*, **12** 052503, 2005.

[19] Parail V V, Energy and Particle Transport in Plasmas with Transport Barriers, *Plasma Phys. Control. Fusion*, **44** A63, 2002.

[20] Tala T J J, Parail V V, Becoulet A, *et al.*, Comparison of Theory-Based and Semi-Empirical Transport Modeling in JET Plasmas with ITBs *Plasma Phys. Control. Fusion* **44** A495, 2002.

[21] Tala T, Laborde L, Mazon D, *et al*, Predictive Transport Simulations of Real-Time Profile Control in JET Advanced Tokamak Plasmas *Nucl. Fusion* **45** 1027, 2005.

[22] Tala T, Imbeaux F , Parail VV, *et al.*, Fully Predictive Time-Dependent Transport Simulations of ITB Plasmas in JET, JT-60U and DIII-D, *Nucl. Fusion*, **46** 548, 2006.

[23] Onjun T, Bateman G, Kritz AH, *et al*., Models for The Pedestal Temperature at The Edge of *H*-mode Tokamak Plasmas, *Physics of Plasmas*, **9** 5018, 2002.

[24] Porcilli F, Boucher D, Rosenbluth MN, Model for The Sawtooth Period and Amplitude, *Plasma Physics and Controlled Fusion*, **38** 2163, 1996.

[25] Bateman G, Nguyen CN, Kritz AH, *et al*., Testing A Model for Triggering Sawtooth Oscillations in Tokamaks, *Physics of Plasmas*, **13** 072505, 2006.

[26] Erba M, Cherubini A, Parail VV, *et al*., Development of A Non-Local Model for Tokamak Heat Transport in *L*-mode, *H*-mode and Transient Regimes, *Plasma Phys. Control. Fusion*, **39** 261, 1997.

[27] Kritz A, Bateman G, Kinsey J, *et al*., The National Transport Code Collaboration Module Library, *Comput. Phys. Comm.*, **164** 108, 2004.

[28] Houlberg WA, Shaing KC, Hirshman SP, *et al*. , Bootstrap Current and Neoclassical Transport in Tokamaks of Arbitrary Collisionality and Aspect Ratio, *Physics of Plasmas*, **4** 3231, 1997.